JOURNAL OF SOLID STATE CHEMISTRY

Volume 179, Number 9, August 2006

CONTENTS

Regular Articles

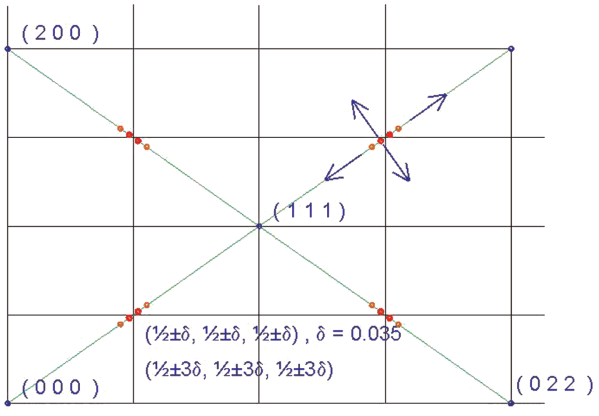

Reciprocal space map of neutron scattering reflections observed for HoB_{12} at 2 K and in zero field. The points show the observed magnetic reflections. The lines show the scan directions.

Regular Articles—Continued

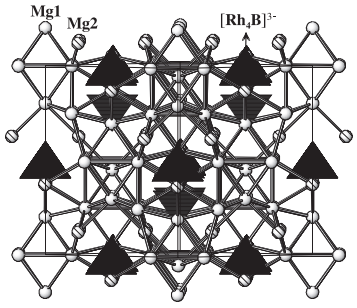

Covalently bonded polyanions $[Rh_4B]^{3-}$ embedded in a cationic matrix in the crystal structure of Mg_8Rh_4B.

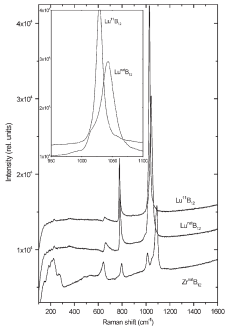

Raman spectra of $Lu^{nat}B_{12}$, $Lu^{11}B_{12}$ and $Zr^{nat}B_{12}$.

Icosahedral B_{12}, macropolyhedral boranes, β-rhombohedral boron and boron-rich solids
Eluvathingal D. Jemmis and Dasari L.V.K. Prasad
Page 2768

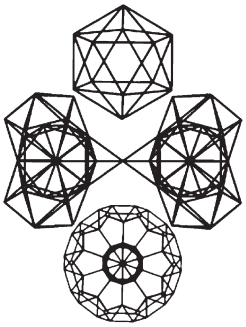

A short legend: Principal building blocks B_{12}, B_{57}, and B_{84} of elemental boron and boron-rich solids.

On the diffusion of free carriers in β-rhombohedral boron
H. Werheit and A. Moldenhauer
Page 2775

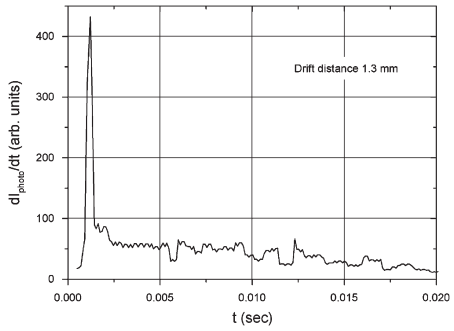

Drift of electron–hole pairs in β-rhombohedral boron.

Portraits of some representatives of metal boride carbide and boride silicide compounds
Mouna Ben Yahia, Jérôme Roger, Xavier Rocquefelte, Régis Gautier, Joseph Bauer, Roland Guérin, Jean-Yves Saillard and Jean-François Halet
Page 2779

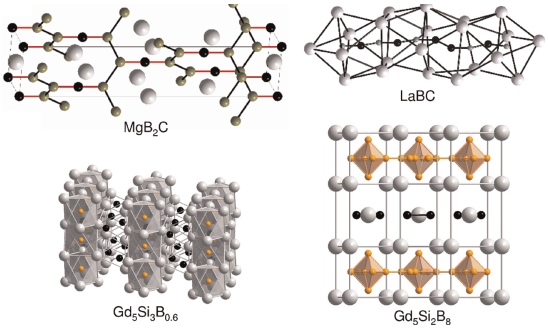

Some ternary alkaline-earth and rare-earth metal boron carbide and silicide compounds are examined using the solid-state language of Zintl–Klemm concept, band structures, and density of states, in order to show that the topology of the non-metal sub-lattice is highly dependent on the electron count.

Differential thermal analysis of the Al + 20% (Fe–50%B) system
J. Abenojar, F. Velasco and M.A. Martinez
Page 2787

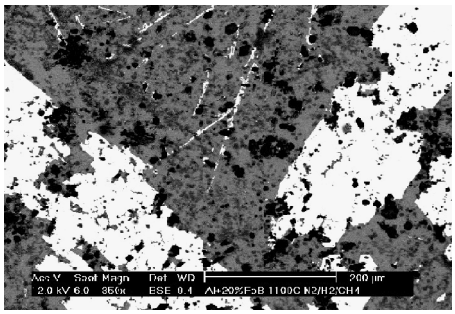

Al + 20%(Fe–50%B) sintered at 1100 °C.

Unusual properties of icosahedral boron-rich solids
David Emin
Page 2791

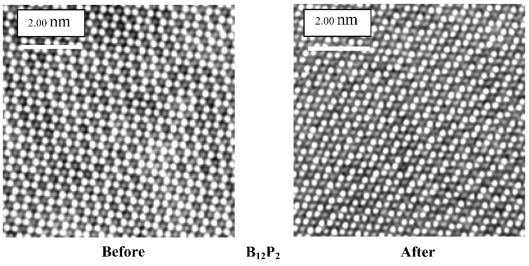

Very high-resolution transmission electron microscopy shows no damage to $B_{12}P_2$ after an intense bombardment (10^{18} electrons/cm^2 s) by 400 keV electrons to a net dose of about 10^{23} electrons/cm^2.

Mg-doping experiment and electrical transport measurement of boron nanobelts
K. Kirihara, H. Hyodo, H. Fujihisa, Z. Wang, K. Kawaguchi, Y. Shimizu, T. Sasaki, N. Koshizaki, K. Soga and K. Kimura
Page 2799

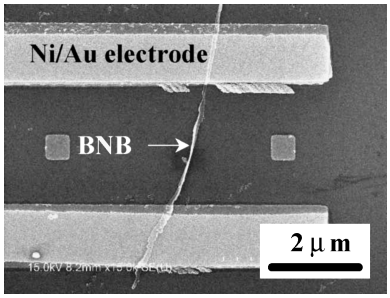

SEM micrographs of boron nanobelt after Ni/Au electrode fabrication by electron beam lithography.

Continued

Anomalous charge transport in CeB_6
M.I. Ignatov, A.V. Bogach, S.V. Demishev, V.V. Glushkov, A.V. Levchenko, Yu.B. Paderno, N.Yu. Shitsevalova and N.E. Sluchanko
Page 2805

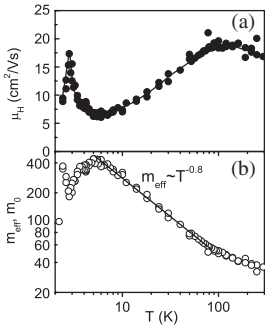

Temperature dependences of the Hall mobility $\mu_H(T)$ and effective mass m_{eff} in CeB_6.

Development and application of high strength ternary boride base cermets
Ken-ichi Takagi
Page 2809

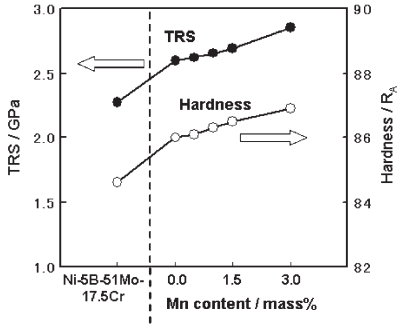

TRS and hardness of Ni–5B–51Mo–17.5Cr and Ni–5B–51Mo–12.5Cr–5V–*x*Mn mass% cermets as functions of Mn content (Fig. 17).

Magnetoresistance and magnetization anomalies in CeB_6
A.V. Bogach, V.V. Glushkov, S.V. Demishev, N.A. Samarin, Yu.B. Paderno, A.V. Dukhnenko, N.Yu. Shitsevalova and N.E. Sluchanko
Page 2819

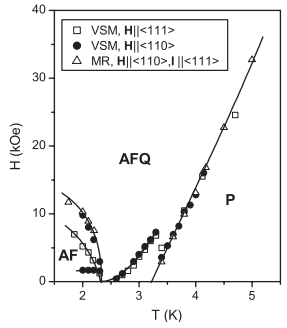

H–T magnetic phase diagram for CeB_6, VSM-data of vibrating sample magnetometer, MR-data of MR measurements. AF, AFQ, P-antiferromagnetic, antiferro-quadrupole, paramagnetic phases correspondingly.

Improvement of thermoelectric properties of alkaline-earth hexaborides
Masatoshi Takeda, Manabu Terui, Norihito Takahashi and Noriyoshi Ueda
Page 2823

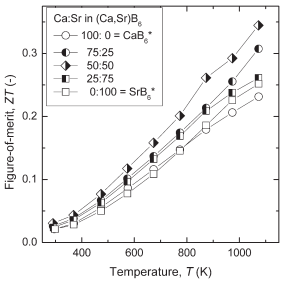

Thermoelectric figure-of-merit, ZT, for (Ca,Sr)B_6 alloys. The highest ZT value of 0.35 at 1073 K was obtained due to effective reduction of thermal conductivity by alloying.

Stability of lithium in α-rhombohedral boron
Wataru Hayami, Takaho Tanaka and Shigeki Otani
Page 2827

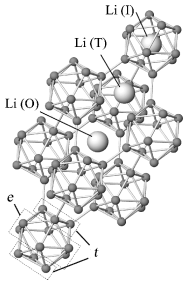

The structure of α-rhombohedral boron. Boron atoms (small spheres) form icosahedra, and the icosahedra form a rhombohedral lattice. Large spheres indicate three possible Li sites, icosahedral (I-), tetrahedral (T-), and octahedral (O-), from top to bottom. The B atoms in an icosahedron are classified into two groups; Six B atoms, denoted by "*t*", that make bonds with neighboring icosahedra, and the other six B atoms denoted by "*e*". This notation was adopted from Ref. [9].

Studies on some ternary oxyborates of the Na_2O–Me_2O_3–B_2O_3 (*Me* = rare earth or aluminum) systems: Synthesis, structure and crystal growth
P. Peshev, S. Pechev, V. Nikolov, P. Gravereau, J.-P. Chaminade, D. Binev and D. Ivanova
Page 2834

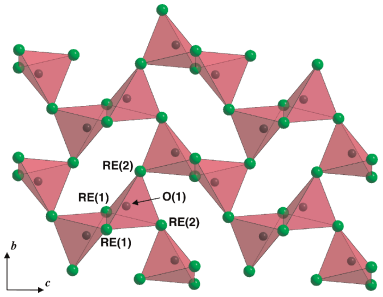

ORE_4 tetrahedra network in $Na_2RE_2O(BO_3)_2$ oxyborates.

Boride-based nano-laminates with MAX-phase-like behaviour
Rainer Telle, Ai Momozawa, Denis Music and Jochen M. Schneider
Page 2850

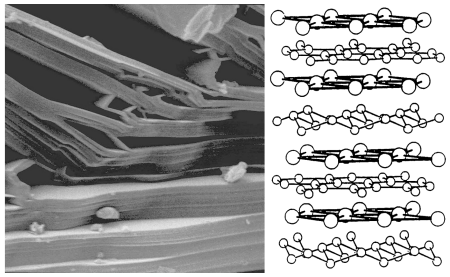

Some transition metal borides crystallise in a layered structure of alternating stacks of metal and boron atoms giving rise for strongly anisotropic properties. Their preferred cleavage parallel and the deformability perpendicular to the basal plan are similar to the peculiar mechanical behaviour recently described for MAX-phases. *Ab initio* calculations of the crystal structure prove the weak bonds between the layers for a variety of borides which can be used to reinforce ceramic materials on a nano-scale level.

Spin-gap magnetic response in (Yb, Lu)B_{12}
E.V. Nefeodova, P.A. Alekseev, J.-M. Mignot, K.S. Nemkovski, V.N. Lazukov, I.P. Sadikov, Yu.B. Paderno, N.Yu. Shitsevalova and R.I. Bewley
Page 2858

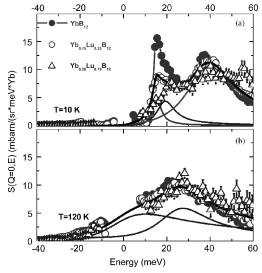

The neutron data indicate that the spin gap is not suppressed by the dilution process even for large Lu concentrations. However, the breakdown of the Yb-sublattice periodicity leads to a strong smearing of the low-energy features and to a moderate suppression of the high-energy peak in the magnetic spectral response of YbB_{12}.

Deposition and investigation of lanthanum–cerium hexaboride thin films
A.S. Kuzanyan, S.R. Harutyunyan, V.O. Vardanyan, G.R. Badalyan, V.A. Petrosyan, V.S. Kuzanyan, S.I. Petrosyan, V.E. Karapetyan, K.S. Wood, H.-D. Wu and A.M. Gulian
Page 2862

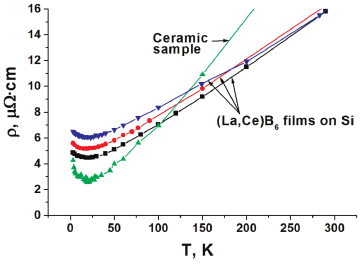

Kondo scattering in $(La,Ce)B_6$ films: temperature dependence of the resistivity of $(La,Ce)B_6$ films on various substrates and the ceramics $La_{0.99}Ce_{0.01}B_6$.

An observation of electron phase transition in SmB_6 at low temperatures
V.V. Glushkov, S.V. Demishev, M.I. Ignatov, Yu.B. Paderno, N.Yu. Shitsevalova, A.V. Kuznetsov, O.A. Churkin, D.N. Sluchanko and N.E. Sluchanko
Page 2871

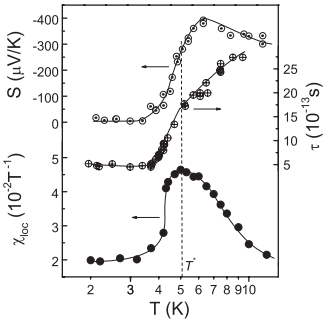

Local susceptibility $\chi_{loc}(T)$, relaxation time $\tau(T)$ and Seebeck coefficient $S(T)$ observed in SmB_6 in the vicinity of $T^* \sim 5$ K (solid lines are guides for eye).

The morphology of ceramic phases in B_xC–SiC–Si infiltrated composites
S. Hayun, N. Frage and M.P. Dariel
Page 2875

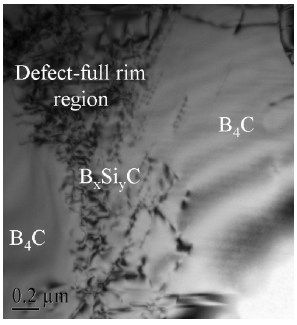

Bright field TEM image of the rim area between two boron carbide grains.

In_3Ir_3B, In_3Rh_3B and $In_5Ir_9B_4$, the first indium platinum metal borides
Wilhelm Klünter and Walter Jung
Page 2880

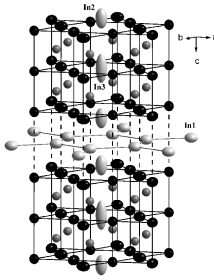

The crystal structure of $In_5Ir_9B_4$ (thermal ellipsoid representation; black: Ir, dark gray: B) is derived from the $CeCo_3B_2$ type and may be interpreted as a layer as well as a channel structure.

Continued

Effect of transition metal doping and carbon doping on thermoelectric properties of YB_{66} single crystals
Takao Mori and Takaho Tanaka
Page 2889

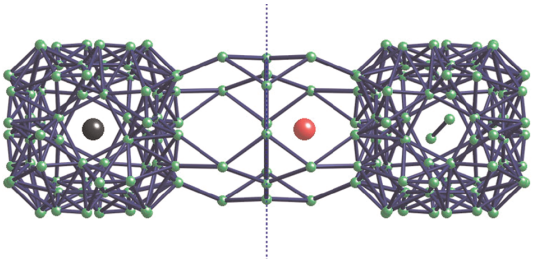

View of the structure of Nb-doped YB_{66} around the doping site of (1/4,1/4,1/4). Boron atoms (green circles), yttrium atom (red circle) and Nb atom (black circle) are displayed. The Nb atom replaces a short B–B dumbbell pair.

Lattice dynamics in the Kondo insulator YbB_{12}
K.S. Nemkovski, P.A. Alekseev, J.-M. Mignot, A.V. Rybina, F. Iga, T. Takabatake, N.Yu. Shitsevalova, Yu.B. Paderno, V.N. Lazukov, E.V. Nefeodova, N.N. Tiden and I.P. Sadikov
Page 2895

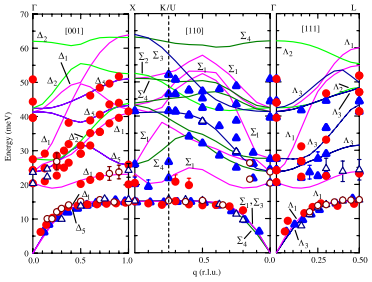

Energy dispersion of phonons in the Kondo insulator YbB_{12} (open symbols) and its structure analogue LuB_{12} (closed symbols). Circles: longitudinal branches; triangles: transverse branches. Lines represent the result of the model calculation based on assumption of a strong hierarchy of the interactions between boron and rare-earth (RE) atoms: B-b $\gg$ B-*RE* $\gg$ *RE-RE*. Irreducible representations of phonon branches are given in the Bouckaert–Smoluchowski–Wigner notation.

Synthesis, crystal growth and structure of Mg containing *β*-rhombohedral boron: $MgB_{17.4}$
Volker Adasch, Kai-Uwe Hess, Thilo Ludwig, Natascha Vojteer and Harald Hillebrecht
Page 2900

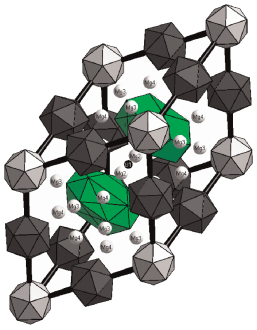

Unit cell of $MgB_{17.4}$ (rhombohedral setting).

Thermoelectric properties of homologous p- and n-type boron-rich borides
T. Mori and T. Nishimura
Page 2908

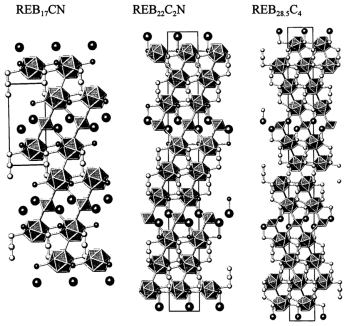

Both p-type and n-type thermoelectric behavior are observed in this homologous boron cluster compound series. This is the first unmodified compound among the boron-rich borides in which n-type behaviour has been observed. Comparative thermal conductivity results indicate the heavy rare earth atoms residing in the boron matrix play a role to depress thermal conductivity.

Synthesis and crystal structure of MgB_{12}
Volker Adasch, Kai-Uwe Hess, Thilo Ludwig, Natascha Vojteer and Harald Hillebrecht
Page 2916

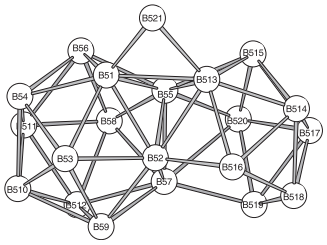

The new crystal structure of MgB_{12} is characterized by a Kagome net of B_{12} icosahedra and B_{21} units, which are observed for the first time. The Mg atoms are placed in voids of the framework.

Ab-initio calculations of Raman, IR-active vibrational modes in isotopically modified B_{12} icosahedral clusters
Naoyuki Nogi and Satoru Tanaka
Page 2927

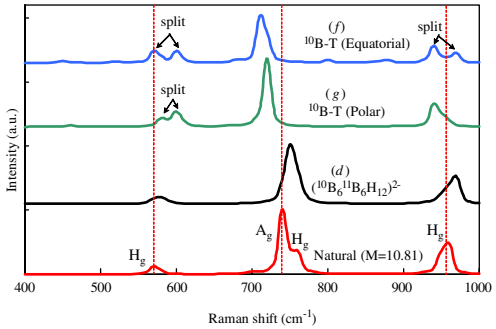

Calculated Raman spectra of the $\{(^{10}B_6{}^{11}B_6)(H_6T_6)\}^2$ anion (*f*)–(*g*) with same isotope ratio. Tritium, T atoms were arranged in the ^{10}B atoms with a rhombohedral arrangement (*f*) and an equatorial (*g*).

Influence of carbon content on physicomechanical characteristics of boron carbide
D. Lezhava, G. Darsavelidze, D. Gabunia, O. Tsagareishvili, M. Antadze and V. Gabunia
Page 2934

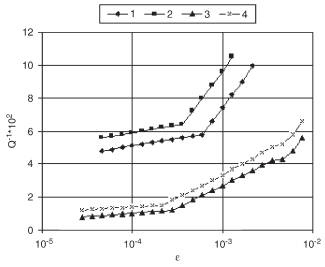

Amplitude dependence of the IF of the compacted samples of boron carbide: $B_{4,3}C$ initial—(1) and after annealing at the 1773 K, 5 h—(2); $B_{6,5}C$ initial—(3) and after annealing at the 1773 K, 5 h—(4).

The directional crystallization of W–B–C–*d*-transition metal alloys
Yuriy Paderno, Varvara Paderno, Alfred Liashchenko, Volodymyr Filipov, Alina Evdokimova and Anna Martynenko
Page 2939

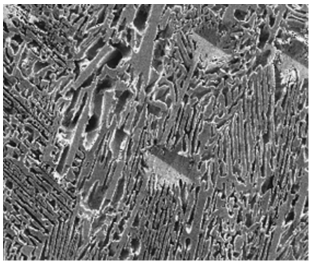

The eutectic structure in WC–WB system.

Peculiarities of changes of some physicomechanical characteristics of monoisotopes ^{10}B, ^{11}B and natural *β*-boron
D. Gabunia, O. Tsagareishvili, D. Lezhava, L. Gabunia, M. Antadze, G. Darsavelidze and T. Tanaka
Page 2944

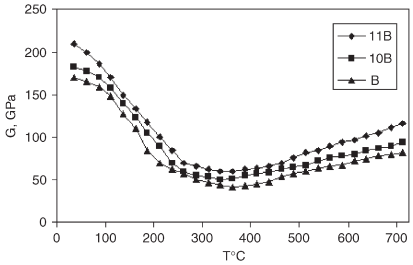

Temperature dependence of the SM in the samples of natural boron B, ^{10}B and ^{11}B monoisotopes.

Preparation and some properties of ScB_2 single crystals
G. Levchenko, A. Lyashchenko, V. Baumer, A. Evdokimova, V. Filippov, Yu. Paderno and N. Shitsevalova
Page 2949

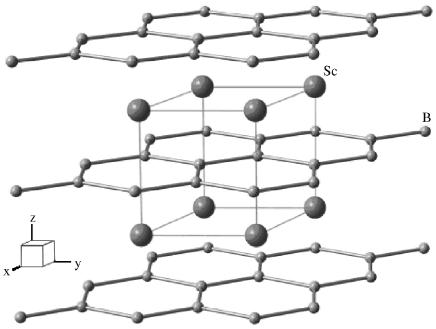

The ScB_2 crystal structure.

X-ray powder diffraction studies and thermal behaviour of $NaK_2B_9O_{15}$, $Na(Na_{.17}K_{.83})_2B_9O_{15}$, and $(Na_{.80}K_{.20})K_2B_9O_{15}$
R. Bubnova, B. Albert, M. Georgievskaya, M. Krzhizhanovskaya, K. Hofmann and S. Filatov
Page 2954

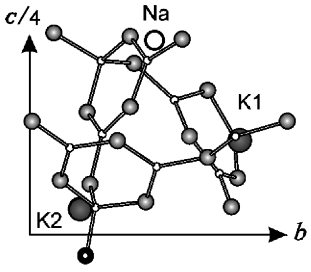

Asymmetrical unit of the $NaK_2B_9O_{15}$ crystal structure.

NOTICE

The Keyword Index for Volume 179 will appear in the December 2006 issue as part of a cumulative index for the year 2006.